where the λ_i's are Lagrange multipliers. The extrema are determined from the following system of equations:

$$\frac{\partial W}{\partial \mu_1} = l_1 - \lambda_1 \cot \alpha_1 = 0 \tag{7}$$

$$\frac{\partial W}{\partial \mu_2} = l_2 + \lambda_1 \cot \Phi_2 - \lambda_2 \cot(\alpha_2 + \Phi_2) = 0 \tag{8}$$

$$\frac{\partial W}{\partial \mu_i} = l_i - \lambda_i \cot(\alpha_i + \Phi_i) + \lambda_{i-1} \cot \phi_i = 0 \quad (i = 3, \ldots, n) \tag{9}$$

$$\frac{\partial W}{\partial \Phi_i} = -\lambda_{i-1}/\sin^2 \Phi_i + \lambda_i/\sin^2(\alpha_i + \Phi_i) = 0 \quad (i = 2, \ldots, n) \tag{10}$$

$$\frac{\partial W}{\partial \lambda_i} = 0 \; (i = 1, \ldots, n) \quad \text{(constraint equations)} \tag{11}$$

Since we have not included the inequality constraints (4–6) in the function W, solutions to Eqs. (7–11) must be checked to satisfy these inequalities. This is easily done in the computation. Indeed, the advantage of this method is that it decouples the μ_i's and the Φ_i's, and allows one to compute sequentially the Φ_i's starting at Φ_2 up to Φ_n, and to compute the optimum μ_i's, starting at μ_n down to μ_1. The algorithm is as follows: 1) Solve Eq. (7) for λ_1. 2) Solve Eqs. (8) and (10) with $i = 2$ for λ_2. 3) Solve Eqs. (9) and (10) with $i = 3, \ldots, n$ for λ_i. 4) Solve Eqs. (11) for $i = n$ to 1 to get the optimum μ_i's: $\mu_n{}^*$, $\mu_{n-1}{}^*, \ldots, \mu_1{}^*$.

However, Eqs. (9) and (10) are transcendental and they yield several solutions. It can be shown[4] that at each step we have two solutions for Φ_i, one negative and the other positive. According to inequality (4), the latter one only corresponds to the solution.

3. Application: Comparison of continuous and Piecewise Optimization

We have considered a rod clamped at one end, supporting a concentrated mass at the other. The continuous optimum design for a specified fundamental frequency has been explained by the authors already mentioned. One may wonder, however, what is the relationship between that continuous design and piecewise uniform designs in which the rod is divided in n uniform regions of equal lengths.

Computation was carried out, using the algorithm of Sec. 2 for $n = 2, 3, \ldots, 10$. Figure 2 shows the ratio $r = \mathcal{M}_o/\mathcal{M}_n$, where $\mathcal{M}_n$ is the structural mass for an n-steps solution and $\mathcal{M}_o$, the corresponding one for the continuous optimum solution. It can be noticed that convergence of the piecewise uniform to the continuous design is rather good and that little is gained by increasing the numer of steps beyond 2 or 3.

Conclusion

The method described here takes advantage of the simplicity of the equations relative to axial (or torsional) vibration. Thus, it has no claim to generality. It has been applied in Ref. 4, however, to the flexural vibration problem of similar mechanical systems. Because of the higher order equations, a numerical iterative scheme had to be used. The comparison of continuous and piecewise uniform optimization yielded the same qualitative results as in the axial case.

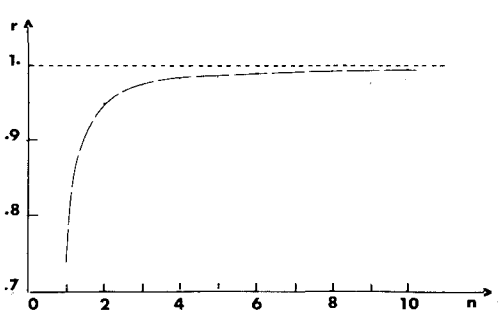

Fig. 2 Ratio $n = \mathcal{M}_o/\mathcal{M}_n$ for $\alpha = \beta L = 1.2$.

References

[1] Turner, M. J., "Design of Minimum Mass Structures with Specified Natural Frequencies," *AIAA Journal*, Vol. 5, No. 3, March 1963, pp. 406–412.

[2] Sheu, C. Y., "Elastic Minimum-Weight Design for Specified Fundamental Frequency," *International Journal of Solids and Structures*, Vol. 4, No. 10, Oct. 1968, pp. 953–958.

[3] Sippel, D. L. and Warner, W. H., "Minimum-Mass Design of Sandwich Structures under a Frequency Constraint," *AIAA Journal*, Vol. 11, No. 4, April 1973, pp. 483–489.

[4] Cardou, A., "Minimum Mass Structural Design with a Frequency Requirement," Ph.D. thesis, March 1972, Univ. of Minnesota, Minneapolis, Minn.

Transient Stresses in Laminated Structures

YING-SAN LAI*
Chicago Bridge and Iron Co, Oak Brook, Ill.

Introduction

THE rapid application of surface pressures to a deformable body gives rise to waves which propagate into the interior of the body. The pattern of propagating stress waves in a laminated structure is rather complicated due to multiple reflections and refractions at the interfaces of the laminates, as well as due to multiple reflections at the external boundaries. These repeatedly reflected and refracted stress waves may in fact combine in phase to generate rather high tensile stresses in the interior to cause the delamination failure. Therefore, it is important to perform detail stress analysis on dynamic laminated structure to ascertain that there will be no undesirable high tensile stresses in the interior of the structure.

The analysis of certain classes of the laminated structures can be simplified by representing the mechanical behavior of a laminated medium by a homogeneous continuum model. The simplest homogeneous continuum model is provided by the effective modulus theory.[1,2] For laminated structures subjected to sharp pulse, however, due to the dynamic stresses in a laminated medium is very sensitive to parameters such as pulse shape, the number of layers, the layer thicknesses, the arrangement of laminations, and the material properties, it is necessary to analyze all layers separately in order to arrive at valid results. In this Note numerical results for two multilayered stress-wave attenuators were presented to verify this effect.

Stress-Wave Attenuators

The stress-wave attenuators which are considered here are multilayered slabs with three main elements: a layer of laminated composite, a layer of adhesive, and a back-up plate. The geometries are shown in Fig. 1. The layer of the laminated composite is fabricated from alternating laminates of two different isotropic homogeneous elastic materials. The subscripts 1 and 2 label the field quantities in the layer made of material 1 and in the layer made of material 2, respectively. The field quantities in the adhesive layer and in the back-up plate are labeled by subscripts 3 and 4, respectively. Perfect bond is assumed at the interfaces.

Referring to Fig. 1, the only difference between the design A and the design B is that in the design A the first layer of the

Received February 13, 1973; revision received July 27, 1973.
Index categories: Structural Composite Materials; Structural Design, Optimal; Structural Dynamic Analysis.

* Presently Chief Stress Analyst, Dresser Industrial Valve & Instrument Division, Alexandria, La.

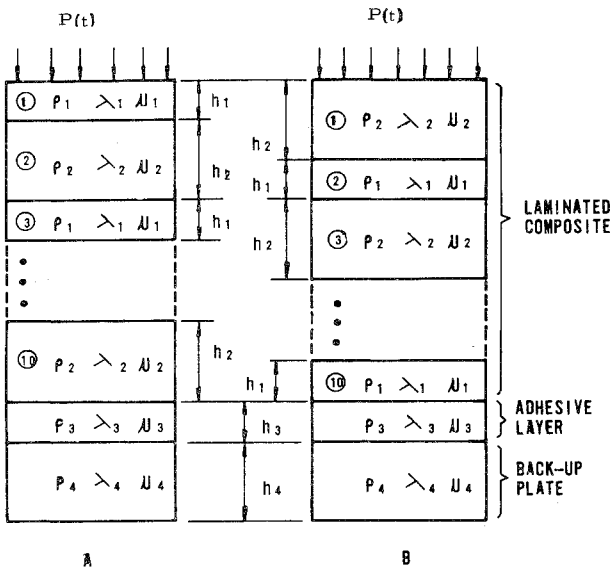

Fig. 1 Stress-wave attenuators.

laminated composite is made of material 1, while in the design B the first layer of the laminated composite is made of material 2. All other design parameters are identical for both designs. The numerical results presented in the next section will show that the transient stress waves propagations in design A and in design B are quite different.

Numerical Procedures and Results

For numerical illustrations, the stress-wave attenuators as shown in Fig. 1 are fabricated from the materials of the properties and thicknesses shown in Table 1. The structures are subjected to the loading $p(t)$ as shown in Fig. 2. The transient stresses in the structures are conveniently computed numerically by means of the method of characteristics. The numerical procedures are described as follows.

Table 1 Properties and thicknesses of the laminates

	ρ (lb/in.^{3})	E (psi)	ν	h (in.)
Laminated composite:				
Material 1	0.065	0.5×10^6	0.35	0.05
Material 2	0.045	6×10^6	0.30	0.10
Adhesive layer:	0.065	0.5×10^6	0.35	0.05
Back-up plate:	0.098	10×10^6	0.34	0.20

Assuming here that the $p(t)$ is uniformly applied, the waves are one-dimensional in nature, and are governed by wave equations of the type

$$\partial^2 u/\partial x^2 - (1/c^2)(\partial^2 u/\partial t^2) = 0 \tag{1}$$

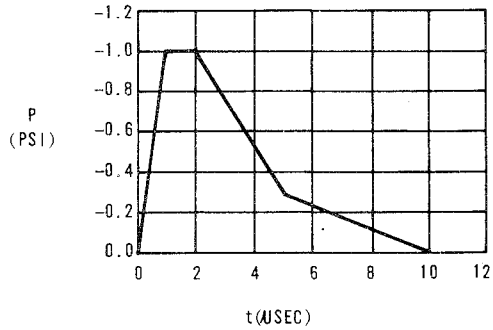

Fig. 2 Pressure pulse.

where the wave velocity c is expressed as

$$c = [(\lambda+2\mu)/\rho]^{1/2} \tag{2}$$

The medium is at rest prior to time $t = 0$. The boundary conditions are

at loading surface $\sigma = -p(t)$ (3)

at free surface $\sigma = 0$ (4)

where the stress σ is related to the displacement as

$$\sigma = (\lambda+2\mu)(\partial u/\partial x) \tag{5}$$

Across the interfaces the tractions and the displacements must be continuous. Thus at any interface between materials 1 and 2 the following relationships hold

$$(\sigma)_1 = (\sigma)_2 \tag{6}$$

$$(v)_1 = (v)_2 \tag{7}$$

where $v = \partial u/\partial t$ is the particle velocity.

For the one-dimensional wave equation, Eq. (1), the characteristic lines are defined by

$$c^+ \text{ characteristic } dx/dt = +c \tag{8}$$

$$c^- \text{ characteristic } dx/dt = -c \tag{9}$$

where c is wave velocity as defined in Eq. (2). The pair of ordinary differential equations along the characteristic lines are derived as

$$\text{along } c^+ \text{ characteristics: } d\sigma - (\rho c)\cdot dv = 0 \tag{10}$$

$$\text{along } c^- \text{ characteristics: } d\sigma + (\rho c)\cdot dv = 0 \tag{11}$$

Let α and β denote the constants for the characteristic lines c^+ and c^-, respectively, the following relations are obtained by integrating Eqs. (10) and (11)

$$\alpha = \sigma - (\rho c)v \tag{12}$$

$$\beta = \sigma + (\rho c)v \tag{13}$$

$$\sigma = (\alpha+\beta)/2 \tag{14}$$

$$v = -(\alpha-\beta)/(2\rho c) \tag{15}$$

Therefore, once σ and v are known at one nodal point (intersection of c^+ and c^- characteristic lines) in the space-time domain (x-t plane), the constants α and β for the two characteristic lines passing through that nodal point can be evaluated from Eqs. (12) and (13). Similarly, once the constants α and β of the two characteristic lines passing through a nodal point in the x-t plane are known then the magnitudes of σ and v at the nodal point can be computed from Eqs. (14) and (15). By alternately employing Eqs. (12–15), the complete solution in the x-t plane can be computed in terms of the prescribed initial conditions and the boundary conditions.

The pattern of propagating stress waves in a laminated medium is extremely complicated. For the purpose to demonstrate that the stress propagation in design A is different from that in design B, it is sufficient to consider any one common location in the structures. Here, the location at the midsurface of the adhesive layer was chosen. The stress variations at the midsurface of the adhesive layers were plotted as functions of time in Fig. 3 for both designs. It can be seen in Fig. 3 that the pattern of wave propagation in design A is substantially different from that in design B. During the first 40 μsec, the maximum tensile stress in design A is 1.23 psi, while in design B, the maximum tensile stress is 0.95 psi. The difference in the maximum stresses is about 30% between two laminated structures with different arrangement of laminations otherwise identical design. Note that in design A the maximum tensile stress is 23% higher than the maximum amplitude of the input pulse while in design B it is 5% lower. It was shown in Ref. 3 that the dynamic stresses in laminated structures can be substantially reduced by optimization process.

Conclusions

For laminated structures subjected to transient pressure pulse, it is necessary to analyze all layers separately in detail. The approximate approach by representing the laminated medium by a homogeneous, transversely isotropic medium will not yield

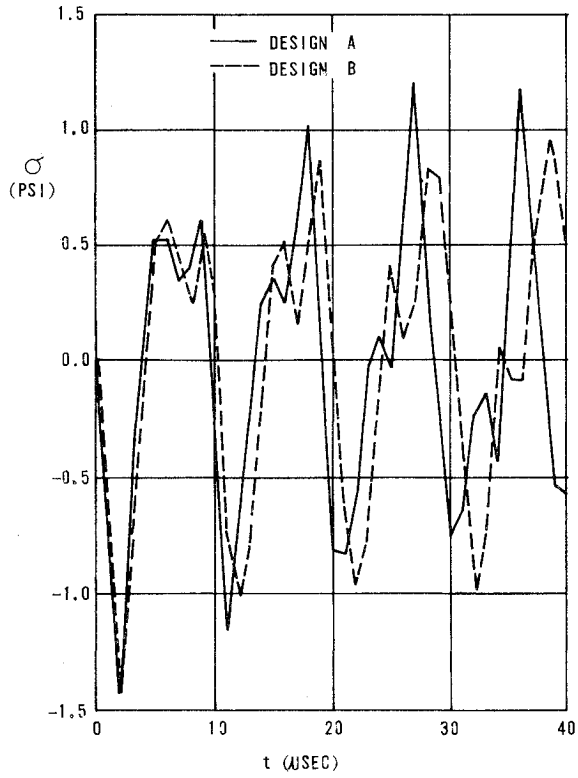

Fig. 3 Stresses at the midsurface of the adhesive layer.

meaningful results. The numerical solutions also reveal the fact that the improperly designed multilayered construction will not produce stress wave attenuation.

References

[1] Postma, G. W., "Wave Propagation in a Stratified Medium," *Geophysics*, Vol. 20, Oct. 1955, pp. 780–806.

[2] Achenbach, J. D. and Zerbe, T. R., "Flexural Vibrations of Laminated Plate," *Journal of the Engineering Mechanics Division, ASCE*, Vol. 97, June 1971, pp. 619–628.

[3] Lai, Y. S. and Achenbach, J. D., "Optimal Design of Layered Structures under Dynamic Loading," *Computers and Structures*, Vol. 3, May 1973, pp. 559–572.

Sweep Effects on Supersonic Separated Flows—A Numerical Study

M. J. WERLE,* V. N. VATSA,† AND S. D. BERTKE†
University of Cincinnati, Cincinnati, Ohio

Introduction

IN the past several years, considerable success has been achieved in numerically solving the two-dimensional laminar boundary-layer equations when separation occurs in supersonic flow.[1-5] To date, only a relatively few papers have appeared which address the three-dimensional separation problem due to the highly complex nature of the flowfield. Contained herein is a brief report on recent successes achieved in the numerical solution of the laminar boundary-layer equations for flow past a swept compression ramp in a Mach 3 freestream. The purposes of this study were to assess the influence of boundary-layer cross flow on the numerical algorithm used for two-dimensional separated flows,[4] to take a first step at extending the two-dimensional separated boundary-layer/inviscid flow interaction model to three dimensions, and to inspect the influence of cross flow on heat-transfer levels in the separation and reattachment regions. The approach taken here is wholly numerical, with finite-difference solutions to the boundary-layer equations (modified to account for interaction with inviscid stream) presented for angles of sweep of 0°, 20°, and 45°.

Received April 12, 1973; revision received July 9, 1973. This research was supported by the Aerospace Research Laboratories under Contract F33615-73-C-4014 and the Naval Air Systems Command under Contract N00019-72-C-0136.

Index categories: Boundary Layers and Convective Heat Transfer—Laminar; Jets, Wakes, and Viscid-Inviscid Flow Interactions.

* Associate Professor, Department of Aerospace Engineering. Associate Member AIAA.

† Research Assistant, Department of Aerospace Engineering.

Governing Equations

The governing equations employed are the classical three-dimensional equations here simplified for constant cross flow and written in terms of the nondimensional Levy-Lees type variables (see Ref. 6 for the nondimensionalization scheme)

$$\xi = \int_0^s \rho_e \mu_e U_e \, ds \qquad \eta = \frac{U_e}{(2\xi)^{1/2}} \int_0^N \rho \, dN \tag{1}$$

and the dependent variables

$$F = u/U_e, \quad G = w/W_e, \tag{2a}$$

$$\theta = T/T_e, \quad l = \rho\mu/\rho_e \mu_e \tag{2b}$$

The governing equations become[6]

Longitudinal momentum:

$$(lF_\eta)_\eta - VF_\eta + \beta(\theta - F^2) - 2\xi F F_\xi = 0 \tag{3a}$$

Cross Flow momentum:

$$(lG_\eta)_\eta - VG_\eta - 2\xi F G_\xi = 0 \tag{3b}$$

Energy:

$$(l\theta_\eta)_\eta/Pr - V\theta_\eta + \alpha_1 F_\eta^2 + \alpha_2 G_\eta^2 - 2\xi F \theta_\xi = 0 \tag{3c}$$

Continuity:

$$V_\eta + F + 2\xi F_\xi = 0 \tag{3d}$$

The viscosity function l is given by Sutherland's law and the inviscid parameters, β, α_1, and α_2 are defined as

$$\beta = (2\xi/U_e) dU_e/d\xi \tag{4a}$$

$$\alpha_1 = (1 - 1/\gamma) U_e^2/T_e, \quad \alpha_2 = (1 - 1/\gamma) W_e^2/T_e \tag{4b}$$

These latter quantities depend on the boundary-layer solution through the interaction of the viscous layer growth with the inviscid streamlines. In essence, the boundary layer displays an "effective body" shape—the displacement surface—to the inviscid mainstream over which the inviscid properties must be computed. For present purposes, linearized supersonic flow with constant cross flow is used to relate the local pressure to the slope of the displacement surface ϕ through the relation

$$p_e = p_\infty + \frac{\cos^2 \Lambda}{(M_\infty^2 \cos^2 \Lambda - 1)^{1/2}} \phi \tag{5}$$

where $\tan \Lambda = W_e/U_e$ is the sweep angle. The isentropic relations provide the remaining inviscid edge quantities and it remains only to relate ϕ to the boundary-layer growth. The total surface inclination includes that induced by the boundary layer as added to the local surface value. In this study, an analytical compression ramp (as shown in Fig. 1) was employed as a "smoothed" version of the typical wedge type configuration employed in experimental separation studies. The ramp angle of approximately 11° was used here since the zero sweep solutions were already available for comparison in Ref. 4. To formally determine the contribution of the boundary-layer growth to the displacement surface angle ϕ, arguments originating in higher order boundary-layer theory are invoked. For regions of nonseparated flows, extension of higher order boundary-layer theory to three dimensions can be shown to locate the inviscid stream surface at a small distance from the surface which exactly corresponds